Development of Current-Fed ICPT System with Quasi Sliding Mode Control

Xiao LV
College of Automation
Chongqing University
No.174, Shazheng Street, Shapingba District, Chongqing
PEOPLE'S REPUBLIC OF CHINA
Lvxiao87@126.com

Yue SUN
College of Automation
Chongqing University
No.174, Shazheng Street, Shapingba District, Chongqing
PEOPLE'S REPUBLIC OF CHINA
syue06@cqu.edu.cn

Zhi-hui WANG
College of Automation
Chongqing University
No.174, Shazheng Street, Shapingba District, Chongqing
PEOPLE'S REPUBLIC OF CHINA
wzhcqu@hotmail.com

Chun-sen TANG
College of Automation
Chongqing University
No.174, Shazheng Street, Shapingba District, Chongqing
PEOPLE'S REPUBLIC OF CHINA
cstang@cqu.edu.cn

Abstract: - In current-fed inductively coupled power transfer (ICPT) systems, voltage distortions and current spikes are easily caused on the semiconductor switches especially when system-parameters vary. This increases the EMI level of the system and the switching loss as well. A quasi sliding mode control (QSMC) method is proposed to improve the dynamic performance of the system by optimization of frequency response. A mathematic model of the system is built up with stroboscopic mapping method and fixed-point theory is applied to get the accurate zero voltage switching (ZVS) frequency. Because of the phase delay caused by the feedback, control and driving circuits, an equivalent model for primary converter is built to figure out the time of phase compensation. Then the QSMC strategy is presented and implemented in developing a prototype current-fed ICPT system. Experimental test results have verified that the proposed control method can regulate the transition of the system to be smooth against wide parameters variations and the spikes on switches have been eliminated effectively.

Key-Words: - Inductively coupled power transfer, Quasi sliding mode control, Frequency response, Zero voltage switching, Stroboscopic mapping

1 Introduction

Inductively coupled power transfer (ICPT) technology is a novel, practical and flexible technology developed to deliver power efficiently from stationary power supply to one or more movable loads utilizing electromagnetic induction principle, modern power electronics, magnetic coupling, high-frequency conversion technology and modern control theory. This technique not only meets the power demand of movable equipment flexibly, safety and efficiently, but also avoids the potential safety hazards exist in the traditional contact power supply systems [1-5]. So, ICPT technology has recently become a worldwide research hotspot.

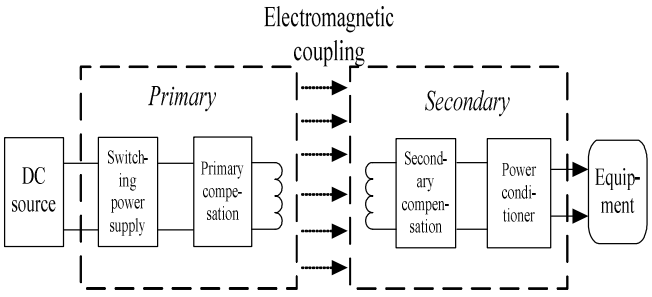

Fig.1. Structures of ICPT system

As shown in Fig.1, the primary of ICPT system comsists of an inverter and a resonant network. In the current-fed ICPT system, real-time voltage feedback control is used to realize the soft switching control of switches. Nevertheless, it can be seen that, in application, when distance between primary and secondary coil (mutual inductance), load or some other cases change, there will be distortions at the zero-crossing of the primary capacitor waveform, and a shock current of switches too. In this situation, the efficiency of system will become lower, while the switches' temperature will rise quickly, even worse, the switches will be damaged soon, and these seriously influence the stability and robustness of the system. In order to prevent this situation, current-fed inverter usually series blocking diodes for each switch to prevent current flowing in reverse. This method would block power access, and have more loss. Obviously that isn't the best solution. Others use such kind of control, which make the control signal in advance. However, the advanced time is different in different types of switches and circuits. So the control method isn't a universal solution, and hard to achieve the best effect on condition that the turn-off and delay time are not fixed.

The inverter which presents the switching characteristics is a periodic time-varying structure system with serious nonlinear behavior. The control of the common inverter is built by the output instantaneous feedback based on the traditional linear control theory [3], but this method has high distortion and poor dynamic characteristics. As a typical nonlinear control strategy, the sliding mode variable structure control has many fine characteristics, such as fast response, insensitive to parameter varies and disturbance, excellent steady as well as dynamic response. At present, the sliding mode variable structure control is frequently used to control the inverter. The difficulty of the ICPT system is the variability of parameters. For instance the reference input is changed by different operations on different loads. If the parameters have been changed greatly in running, the chattering will occur. However, as a kind of improvement of traditional sliding mode control, the quasi sliding mode control (QSMC) doesn't require switching control structure on the switching surface. This control strategy can transform the structure on the boundary layer, besides it has continuous feedback control without structural transformation. This difference can weaken or avoid the chattering fundamentally [11].

According to these analyses, this paper uses the QSMC strategy to determine the control function for current-fed ICPT system. The system can rapidly enter the soft switching conditions when the parameters of resonant network or load disturbance are changing. The result of experiment shows that the waveforms of system are obviously improved and the robustness is enhanced too. When load changes, the system can rapidly track the parameters change, and always operates at zero voltage switching (ZVS) conditions.

2 Analysis of Distortion

In ICPT system, most of the primary uses the full-bridge inverter as the main circuit of system which is shown in Fig.2. The current-fed ICPT system with parallel resonance has strong current limitation and high reliability for short circuit protection [2], especially applies to the ICPT system with track loop.

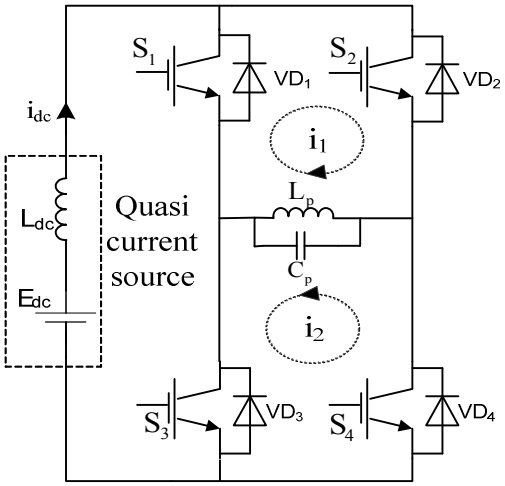

Fig.2. Primary of current-fed ICPT system

For these kinds of systems, the traditional control method is that the output signal is divided into two complementary signals and sent to the gate drives circuit to drive the switches of the resonant circuit [1]. If the control signals of the four switches are interactive conduction, the waveform across capacitor C_p should be standard sinusoidal voltage, nevertheless, the reality is shown in Fig.3. The primary resonant voltage is not standard sine wave with distortions at the zero-crossing point. Moreover, the current waveform of switches is poor-quality with spikes at the zero-crossing point.

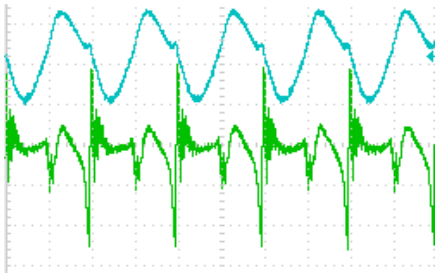

Fig.3. Waveforms of capacitor C_p and current of switches

Generally, there are two reasons to produce such distortion. One is caused by the real-time resonant frequency, which is changed when the load varies. The dynamic property of traditional linear feedback control is so poor that the frequency of the drive signal is not equal to the real-time ZVS frequency. Sometimes, the excessive deviation of frequency probably induces system detuning resulting in serious consequence. The other is due to the phase-shifting between the real-time ZVS signal and the drive signal caused by the delay in the detection or drive part etc. At the zero-crossing point, because of its own induction electromotive force, the primary inductor L_p forms the loop between the switches S_2 and VD_1 or VD_4 and S_3 which is shown in Fig.3. Because of the small internal resistance of switches, even small voltage can produce large current. The existence of this spike current is harmful to switches which may burn out due to the temperature rise rapidly; even worse, the whole system may collapse immediately.

3 Determination of Key Parameters

Base on the previous work, the main distortions are due to the frequency deviation and the phase delay, therefore, it is necessary to determine the two parameters.

3.1 Determine real-time ZVS frequency

There are several methods to calculate the real-time ZVS frequency of circuits such as ac impedance analysis, generalized state space average method, various discrete-time modeling method, and stroboscopic mapping method.

In this paper, the stroboscopic mapping method for accurately determining the steady-state of the resonant frequency is proposed. The essential idea of the method is an extension to the basic stroboscopic mapping theory with the operating period being treated as a variable and fixed point theory being applied to find the resonant frequency of the system.

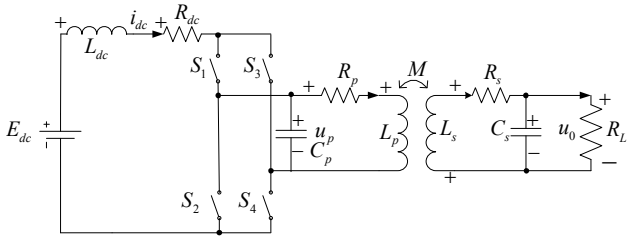

Fig.4. Schematic of current-fed ICPT system

As shown in Fig.4, let the system state vector and input vector be $x=\left[i_{dc},u_p,i_p,i_s,u_s\right]^T$ and $u=\left[E_{dc}\right]$ respectively. Then it could be got that:

$$\begin{cases}\dot{x}=A_1x+B_1u & \mathrm{mod}\,e1\\ \dot{x}=A_2x+B_2u & \mathrm{mod}\,e2\end{cases} \tag{1}$$

and the coefficient matrices are:

$$A_1=\begin{bmatrix}-\frac{R_{dc}}{L_{dc}} & -\frac{1}{L_{dc}} & 0 & 0 & 0\\ \frac{1}{C_p} & 0 & -\frac{1}{C_p} & 0 & 0\\ 0 & \frac{-L_s}{\Delta} & \frac{L_sR_P}{\Delta} & \frac{MR_s}{\Delta} & \frac{M}{\Delta}\\ 0 & \frac{-M}{\Delta} & \frac{MR_P}{\Delta} & \frac{L_pR_s}{\Delta} & \frac{L_p}{\Delta}\\ 0 & 0 & 0 & \frac{1}{C_s} & -\frac{1}{R_LC_s}\end{bmatrix} \tag{2}$$

$$A_2=\begin{bmatrix}-\frac{R_{dc}}{L_{dc}} & \frac{1}{L_{dc}} & 0 & 0 & 0\\ -\frac{1}{C_p} & 0 & -\frac{1}{C_p} & 0 & 0\\ 0 & \frac{-L_s}{\Delta} & \frac{L_sR_P}{\Delta} & \frac{MR_s}{\Delta} & \frac{M}{\Delta}\\ 0 & \frac{-M}{\Delta} & \frac{MR_P}{\Delta} & \frac{L_pR_s}{\Delta} & \frac{L_p}{\Delta}\\ 0 & 0 & 0 & \frac{1}{C_s} & -\frac{1}{R_LC_s}\end{bmatrix} \tag{3}$$

$$B_1=B_2=\begin{bmatrix}\frac{1}{L_{dc}} & 0 & 0 & 0 & 0\end{bmatrix}^T \tag{4}$$

$$\Delta=M^2-L_pL_s \tag{5}$$

Based on the stroboscopic mapping model of steady state with fixed point theory, the system operating period could be described as follows[7]:

$$x^*=\left(1-\Phi_2\left(\frac{T}{2}\right)\Phi_1\left(\frac{T}{2}\right)\right)^{-1}\cdot\Delta_1 \tag{6}$$

where:

$$\Phi_i\left(t\right)=e^{A_it}\qquad i=1,2 \tag{7}$$

$$\begin{aligned}\Delta_1=&\Phi_2\left(\frac{t}{2}\right)\left(\Phi_1\left(\frac{t}{2}\right)-I\right)A_1^{-1}B_1E_{dc}\\ &+\left(\Phi_2\left(\frac{t}{2}\right)-I\right)A_2^{-1}B_2E_{dc}\end{aligned} \tag{8}$$

In order to get the zero-crossing point of the system, choose the u_p of x^*, which can be represented as:

$$Y=\left[0,1,0,0,0\right] \tag{9}$$

Define a fixed-point function as follows:

$$f_{x^*}\left(t\right)=Y\left(1-\Phi_2\left(\frac{t}{2}\right)\Phi_1\left(\frac{t}{2}\right)\right)^{-1}\bullet\Delta_1 \tag{10}$$

All the zero-crossing points of the fixed-point function (10) are corresponding to the ZVS periods of the system. With a numerical calculating method, it is easy to get the non-zero solutions T_1, T_2… T_n of equation $f_{x^*}\left(t\right)=0$. If the system operates at the period T_i (i=1, 2… n), the voltage of up is zero at the switching point, therefore, the T_i (i=1, 2… n) is the real-time ZVS period. In addition, it can be seen that the real-time frequency is related to the load parameter and mutual inductance from the equation(10).

3.2 Determine time of compensation

Fig.2 can be equivalent to the circuit as shown in Fig.5, then it can be obtained a second order differential equation about the voltage u_p across the capacitor C_p.

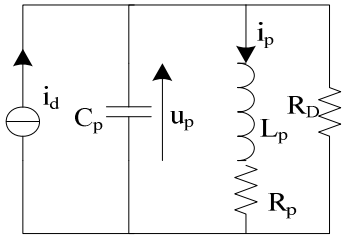

Fig.5. Equivalent circuit diagram for distortion

Then it can be figured out the equation for u_p:

$$u_p = \frac{i_d R_P R_D (1 - e^{\frac{-2t}{C_p \cdot R_p}}) - u_{p0} \cdot (R_D + R_P) \cdot e^{\frac{-2t}{C_p R_p}}}{R_D + R_P} \quad (11)$$

The solution t of equation u_p=0 is the compensative time τ. And the complete solution of τ is:

$$\tau = \frac{C_p R_D R_P \cdot \log(\frac{i_d R_D R_P - R_D u_{p0} - R_P u_{p0}}{i_d R_D R_P})}{R_D + R_P} \quad (12)$$

where R_D is the resistance of the body diode in the switches.

4 Quasi Sliding Mode Control

According to the chapter 3.1, it can be seen that the real-time frequency of the ICPT system varies when the system parameters change such as the load, the mutual inductance. Especially, when the real-time frequency varies greatly, there is an ultrahigh frequency in the frequency transition with the bang-bang control, which can harm the switches. If the PI controller is proposed, the variable real-time frequency may cause system detuning problems. Hence, it is important to improve the control method.

The dynamic response of the sliding mode variable structure control system is divided into two stages, one is the reaching stage which makes the motion from initial state to reaching the switching surface s=0 in limited time. The other is the sliding mode stage which makes the system sliding along the switching surface. The system only in the sliding mode stage has strong robustness. However, the chattering may occur in the sliding mode stage.

The system motion path of QSMC is limited in some Δ neighborhood of the ideal sliding mode. The phase locus of ideal sliding mode control is that the state points in some certain ranges are all drawn to switching surface. But in QSMC the state points are drawn to some Δ neighborhood of switching surface which is usually called the boundary layer of the sliding mode switching surface. Besides, the QSMC has several advantages, such as fast response, insensitive to parametric variable and disturbance, and excellent steady as well as dynamic response. Therefore, this paper proposes a QSMC on ZVS by the dynamic frequency compensation to eliminating the switches' current spike. Especially, when the departure of the drive signal and the real-time ZVS frequency is greatly, the strategy could realize the system transition smoothly and safety.

To eliminating the chattering of system, the QSMC uses the saturation function $sat(s)$ instead of the $sign(s)$ in traditional sliding mode control.

$$sat(s) = \begin{cases} 1 & s > \Delta \\ k's & |s| \le \Delta \\ -1 & s < -\Delta \end{cases} \qquad k' = \frac{1}{\Delta} \quad (13)$$

where Δ is the boundary layer.

The essence of saturation function is that switching control is used beyond the boundary layer while linear feedback control is used within the boundary layer.

Assume $s = f - f_{ref}$ (14)

where f_{ref} is the real-time resonant frequency.

The control function u can be described as the step size of frequency and can be expressed as follow:

$$u = \begin{cases} 1 & s > \Delta \\ s & |s| < \Delta \\ -1 & s < -\Delta \end{cases} \quad (15)$$

where Δ=1kHz.

It can be seen that if the frequency of control signal is higher than the real-time resonant frequency more than 1kHz, the step size is 1kHz for decreasing.

While if the frequency of control signal is less than the real-time resonant frequency more than 1kHz, the step size is 1kHz for increasing. However, if value of difference between the control signal and the real-time resonant frequency is less than 1kHz, the step size is the difference which is lower than 1kHz. The control flow chart is shown in Fig.6.

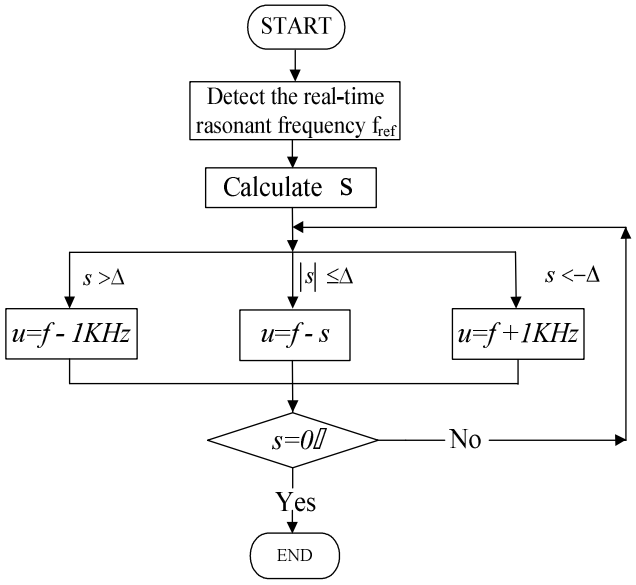

Fig.6. Control flow chart

5 System Implementation

On the basis of above analyses, an ICPT system using QSMC is shown in Fig.7.

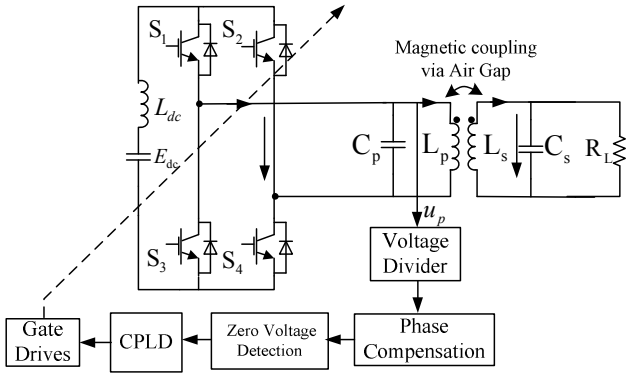

Fig.7. Experimental implementation diagram

From the above figure, it can be known that the system consists of several parts which include the full-bridge inverter, gates drives, voltage divider, phase compensation, zero voltage detector, complex programmable logic device (CPLD) and pick-up parts.

The voltage divider paralleled resistance is used to make the input of phase compensation to be 1% of the voltage of u_p.

The phase compensation is used to compensate the time of delay in circuit. A RC lead network as shown in Fig.8 is designed for compensation which makes control signal ahead of the signal from the voltage divider for a short time.

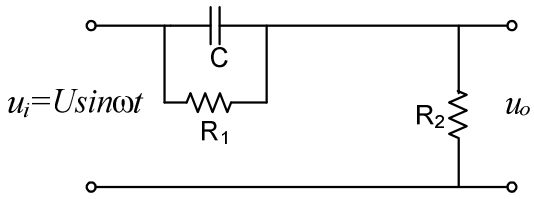

Fig.8. RC lead network

If it is assumed that the input of the lead network is $u_i = U\sin\omega t$, the output of the network can be described as:

$$u_0 = \frac{j\omega R_1^2 R_2 C + \omega^2 R_1^2 R_2^2 C^2 + R_2(R_1+R_2)}{(R_1+R_2)^2 + \omega^2 C^2 R_1^2 R_2^2} U\sin\omega t \quad (16)$$

From the above equation, it can be seen that the output u_o is ahead of the input u_i in phase, the phase angle θ can be described as:

$$\theta = \arctan \frac{\omega R_1^2 C}{\omega^2 R_1^2 R_2 C^2 + R_1 + R_2} \quad (17)$$

Then the time of leading is as follows:

$$t = \frac{\theta}{2\pi} T = \frac{\theta}{2\pi f} = \frac{\theta}{\omega} \quad (18)$$

It can be figured out the values of the parameters in network according to the equation (12) and (18). Nevertheless, the maximal compensate time of this lead network is a quarter period.

The zero voltage detector comprises two high-speed comparators. The LM311 chip is selected as the comparator. Then, the output signal of the zero voltage detector is disposed by CPLD controller which generates the control signals based on the control strategy as shown in Fig.6. Finally, the control signals are sent to the gate drives circuit to

drive the switches of the full-bridge inverter to realizing the ZVS states. CPLD chip (Altera EPM240T100C5N) is selected as controller and the drivers are realized with IR2103 chip. IGBT semiconductors (FGA25N120) are selected as the switches of the full-bridge inverter.

6 Experimental Study

In order to verify the controller results experimentally, an experimental prototype has been set up as shown in Fig.9. The parameters of the example current-fed ICPT system are shown in Table 1.The controller based on the control function u is built in the CPLD.

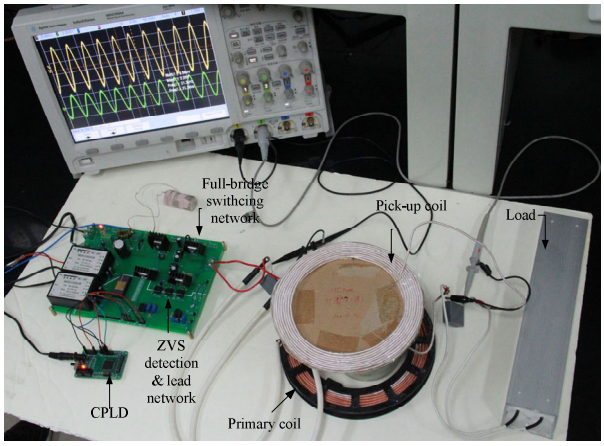

Fig.9. Experimental prototype of the system

Table 1. Parameters of current-fed ICPT system

Parameters	Values
DC input supply E_{dc}	100V
DC inductance L_{dc}	3mH
Primary resonant inductance L_p	360μH
Primary resonant capacitance C_p	0.15μF
Secondary resonant capacitance L_s	155μH
Secondary resonant inductance C_s	0.34μF
Resistance of the primary coil R_P	0.68Ω
Resistance of the by pass diode in switches R_D	0.05Ω

According to Table 1, values of the lead network parameters as shown in Fig.8 are C=1nF, R_1=4.7kΩ, R_2=2.7kΩ. The coils of primary and secondary are wrapped as shown in Fig.9, relation between distance (d) and mutual inductance (M) is measured by digital electric bridge as shown in Table 2.

Table 2. Relationship between d and M

Distance d (cm)	Mutual inductance M (μH)
1	115.7
2	87
3	68.9
4	56.2
5	45
6	37.1
7	29.8
∞	0

The steady state waveforms of the system when d is 5cm and R_L is 100Ω are shown in Fig.10. In Fig.10(a), the primary switches' current i_{ds} and primary resonant voltage u_p waveforms are shown when the system is in the ZVS state. It can be seen that u_p has perfect sinusoidal waveform quality and there is no spike in i_{ds}. The frequency of the ZVS sates which is up to 19.8KHz is in accordance with the theoretical result of the equation (10).

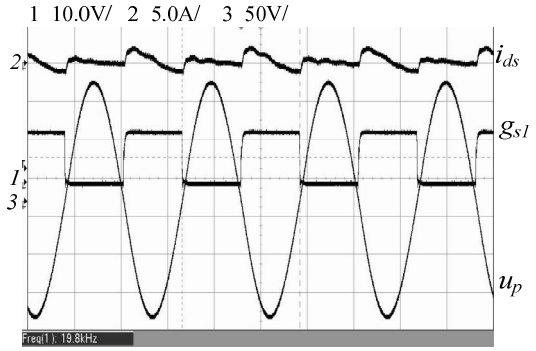

(a) Running in the ZVS state

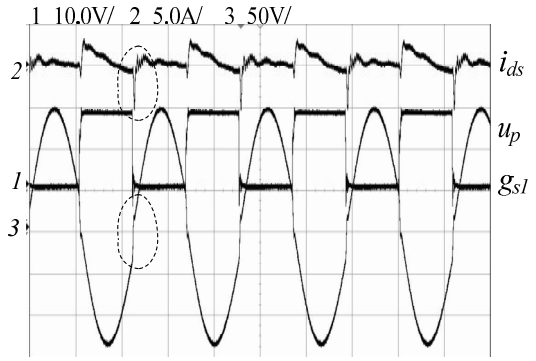

(b) Not in the ZVS state

Fig.10. Steady state waveforms

Compared with the Fig.10(a), Fig.10(b) shows the waveforms of the system which isn't running in the ZVS state. It can be seen that u_p has bad sinusoidal waveform quality and there are serious spikes in i_{ds} at the zero-crossing point.

In order to evaluate the performances of the QSMC system, comparing with the bang-bang control results, the parameters perturbations and the start-up process experiments are all investigated as follows. As shown in Fig.11, the experimental results in load variations are obtained. Fig.11(a) shows the pick-up voltage u_s and the primary switch's current i_{ds} waveforms with load varied from 100Ω to 33.3Ω based on bang-bang control. It can be seen that there is a peak in the i_{ds} when the load varied. While the waveforms based on the QSMC are shown in the Fig.11(b). It can be seen that the responses of i_{ds} are very smooth with the load changing between 100Ω and 33.3Ω. At the same time, the output voltage is changed from 140V to 70V with load varied from 100Ω to 33.3Ω. The output voltage also returns to 140V smoothly when load returns to 100Ω. Likewise, Fig.12 shows waveforms with mutual inductance varied from 45μH to 0μH. It can be obviously seen the QSMC has better control quality than the bang-bang control when mutual inductance varied. Because there is a large frequency shifts, the switches based on bang-bang control have been switched with an ultrahigh frequency when parameters varied.

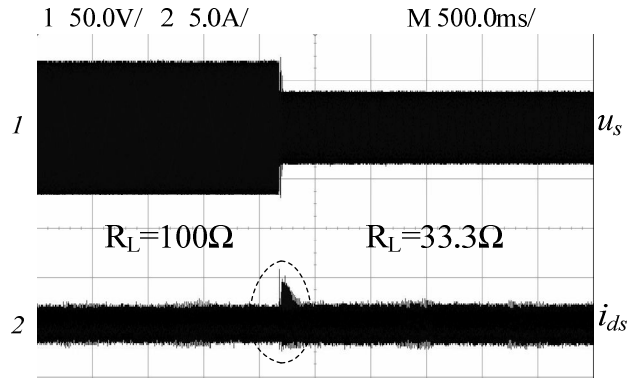

(a) Bang-bang control

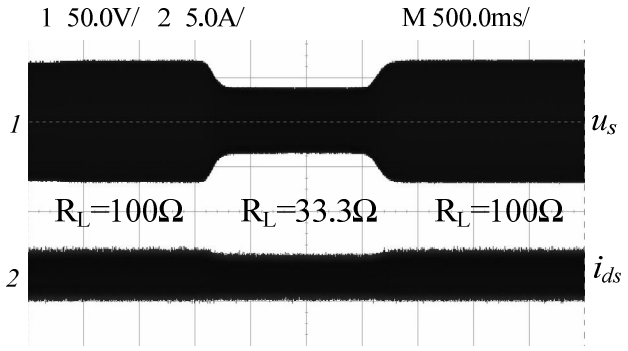

(b) QSMC

Fig.11. Waveforms with load variations

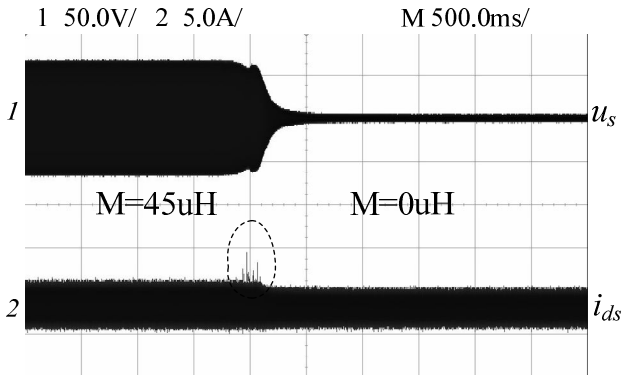

(a) Bang-bang control

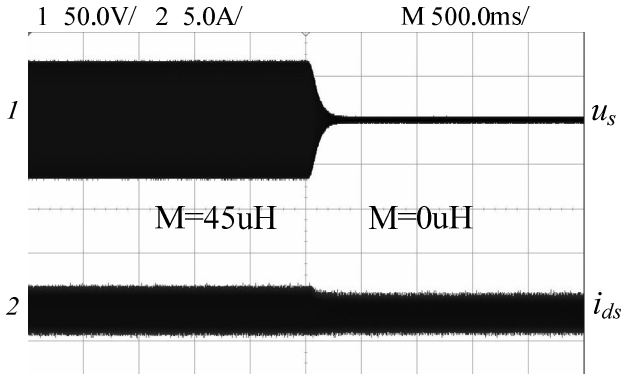

(b) QSMC

Fig.12. Waveforms with mutual inductance variations

Finally, using the two different control strategies, the start-up waveforms are shown in Fig.13. It can be seen that the experimental waveform of i_{ds} has a large spike during the start-up process with bang-bang control as shown in Fig.13(a), nevertheless, Fig.13(b) shows that there is a better start-up process with

QSMC. From these measured waveforms, it is evident that the QSMC system has safe and superior performance.

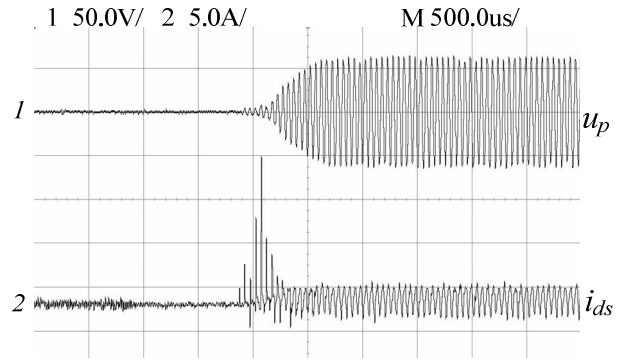

(a) Bang-bang control

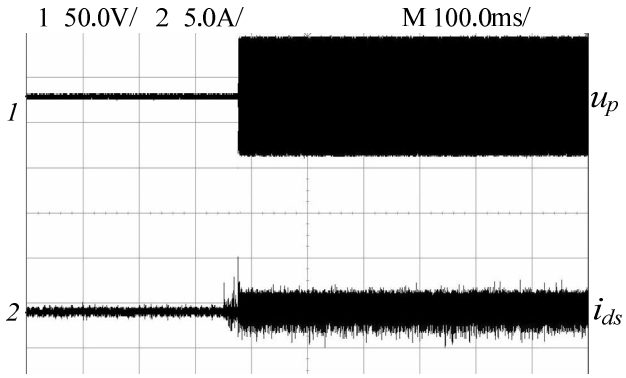

(b) QSMC

Fig.13. Start-up waveforms

From all above analyses, it can be concluded that for current-fed ICPT system, QSMC has achieved the stability and a certain robust performance which is better than that of bang-bang controller, especially from the aspects of resisting the wide parameters variations. In practice, QSMC strategy will be very effective for current-fed ICPT systems with parameter variations.

7 Conclusions

This paper mainly introduces the production principle of distortion in current-fed ICPT system. The real-time resonant frequency is obtained based on a stroboscopic mapping model and fixed-point theory. The compensation time is figured out using equivalent modeling analysis. The proposed system which consists of hardware and the QSMC function is designed. In order to show the necessary of this approach, the QSMC strategy is compared with the bang-bang control system. The experimental results show that the proposed control method provides a better transition process when environmental parameters change greatly.

Acknowledgment

This research work is financially supported by National Natural Science Foundation of China under Grant 51007100 and Fundamental Research Funds for the Central Universities under Grant CDJXS10170002. I also would like to give my special thanks to the anonymous reviewers of this paper for their contributions to this work.

References:

[1] A.P.Hu, Resonant Converter for IPT Power Supplies[D], *New Zealand: Department of Electrical and Electronic Engineering, University of Auckland*, 2001.

[2] A.P.Hu, J.T.Boys and G.A.Covic, Frequency Analysis and Computation of a Current-fed Resonant Converter for ICPT Power Supplies[C], *Proceedings of International Conference on Power System Technology, Perth: IEEE*, 2000, pp. 327– 332.

[3] A.P.Hu, J.T.Boys and G.A.Covic, ZVS Frequency Analysis of a Current-Fed Resonant Converter[C], *Processing of International Power Electronics Congress, IEEE*, 2000, pp. 217-221.

[4] W.Fang, H.J.Tang and W. Liu, Modeling and Analyzing an Inductive Contactless Power Transfer System for Artificial Hearts Using the Generalized State Space Averaging Method[J],

Journal of Computational and Theoretical Nanoscience, vol.4, 2007, pp. 1412-1416. 1015-1018.

[5] TANG Chun-sen, SUN Yue and SU Yu-gang, Determining Multiple Steady-State ZCS Operating Points of a Switch-Mode Contactless Power Transfer System[J], *IEEE. Trans. on Power Electronics*, vol.24, 2009, pp.416-425.

[6] P.Si, A.P.Hu and S. Malpas, A Frequency Control Method for Regulating Wireless Power to Implantable Devices[J], *IEEE Transactions on Biomedical Circuits and Systems*, 2008, pp. 22-29.

[7] TANG Chun-sen, SUN Yue, DAI Xin and SU Yu-gang, Extended Stroboscopic Mapping (ESM) Method: a Soft-Switching Operating Points Determining Approach of Resonant Inverters[C], *Processing of International Conference on Sustainable Energy Technologies, IEEE*, 2010.

[8] Lopez M, Garcia de Vicuna J L and Castilla M, Control Design for Parallel-Connected DC-AC Inverters Using Sliding Mode Control[C], *Processing of IEEE PEVSD*, 2000, pp. 457-460.

[9] X.Liu and S.Hui, Equivalent Circuit Modeling of a Multilayer Planar Winding Array Structure for Use in a Universal Contactless Battery Charging Platform[J], *IEEE Trans. on Power Electronics*, 2007, pp. 21–29.

[10] Y.Sun, A.P.Hu and X.Dai, Discrete Time Mapping Modeling and Bifurcation Phenomenon Study of a ZVS Converter[C], *Processing of Int.Conf. Power Sys. Tech, IEEE*, 2004, pp.

[11] A.Bartoszewicz, Discrete Time Quasi Sliding Mode Control Strategies[J], *IEEE Transactions on Industrial Electronics*, 1998, pp. 633 – 637.

[12] I.E.Colling and I.Barbi, Reversible Unity Power Factor Step-up/Step-down AC-DC Converter Controlled by Sliding Mode[J], *IEEE Trans. on Power Electronics*, 2001, pp. 223 ~ 230.

[13] V.I.Utkin, Variable Structure Systems with Sliding Modes[J], *IEEE Trans. on Automatic Control*, 1977, pp. 212-222.

[14] D.Munoz and D.Sbarbaro, An Adaptive Sliding-Mode Controller for Discrete Nonlinear Systems[J], *IEEE trans. on Industrial Electronics*, Vol.47, 2000, pp. 574-581.

[15] R.Rojas and O.Camacho, On Sliding Mode Control for Nonlinear Electrical Systems[J], *WSEAS Trans. on circuits and systems*, 2004, pp. 783-793.

[16] Ramos and R.R.Biel, A Fixed-Frequency Quasi-Sliding Control Algorithm: Application to Power Inverters Design by Means of FPGA Implementation[J], *IEEE Trans. on Power Electronics*, Vol.18,2003, pp. 344-355.

[17] WANG Feng-yao, The Sliding Mode Variable Structure Control[M], *China Machine Press*, 1998.